Received: 23 July 2020 | Revised: 31 July 2020 | Accepted: 31 July 2020

DOI: 10.1002/pro.3924

THE PROTEIN SOCIETY WILEY

ARTICLE

Domain interactions determine the conformational ensemble of the periplasmic chaperone SurA

Dagan C. Marx[1] | **Mathis J. Leblanc**[1] | **Ashlee M. Plummer**[1,2] | **Susan Krueger**[3] | **Karen G. Fleming**[1]

[1]Thomas C. Jenkins Department of Biophysics, Johns Hopkins University, Baltimore, Maryland

[2]Department of Cell Biology, Harvard Medical School, Boston, Massachusetts

[3]National Institute of Standards and Technology, Gaithersburg, Maryland

Correspondence
Karen G. Fleming, Thomas C. Jenkins Department of Biophysics, Johns Hopkins University, Baltimore, Maryland.
Email: karen.fleming@jhu.edu

Funding information
Division of Chemistry, Grant/Award Number: CHE 1265821; Division of Graduate Education, Grant/Award Number: 1232825; Division of Materials Research, Grant/Award Number: DMR 1508249; Division of Molecular and Cellular Biosciences, Grant/Award Numbers: MCB 1412108, MCB 1931211; Engineering and Physical Sciences Research Council, Grant/Award Number: EP/K039121/1; National Institute of General Medical Sciences, Grant/Award Number: T32 GM008403

Abstract

SurA is thought to be the most important periplasmic chaperone for outer membrane protein (OMP) biogenesis. Its structure is composed of a core region and two peptidylprolyl isomerase domains, termed P1 and P2, connected by flexible linkers. As such these three independent folding units are able to adopt a number of distinct spatial positions with respect to each other. The conformational dynamics of these domains are thought to be functionally important yet are largely unresolved. Here we address this question of the conformational ensemble using sedimentation equilibrium, small-angle neutron scattering, and folding titrations. This combination of orthogonal methods converges on a SurA population that is monomeric at physiological concentrations. The conformation that dominates this population has the P1 and core domains docked to one another, for example, "P1-closed" and the P2 domain extended in solution. We discovered that the distribution of domain orientations is defined by modest and favorable interactions between the core domain and either the P1 or the P2 domains. These two peptidylprolyl domains compete with each other for core-binding but are thermodynamically uncoupled. This arrangement implies two novel insights. Firstly, an open conformation must exist to facilitate P1 and P2 exchange on the core, indicating that the open client-binding conformation is populated at low levels even in the absence of client unfolded OMPs. Secondly, competition between P1 and P2 binding paradoxically occludes the client binding site on the core, which may serve to preserve the reservoir of binding-competent apo-SurA in the periplasm.

Abbreviations and Symbols: BAM, β-barrel assembly machine; CD, circular dichroism; NIST, National Institute of Standards and Technology; OMP, outer membrane protein; PPIase, peptidyl prolyl isomerase; P1, PPIase domain number 1 on SurA; P2, PPIase domain number 2 on SurA; SANS, small-angle neutron scattering; SE, sedimentation equilibrium; smFRET, single-molecule Förster resonance energy transfer; TB, Terrific broth; uOMP, unfolded OMP; client, uOMPs that require SurA for efficient biogenesis.

Karen Fleming is the winner of the 2020 Carl Brändén Award and a Protein Society Member.

KEYWORDS
conformational dynamics, *Escherichia coli* periplasmic chaperones, outer membrane protein biogenesis, SurA protein

1 | INTRODUCTION

Outer membrane proteins (OMPs) play essential roles in gram-negative bacteria such as nutrient uptake,[1] modifying lipid structures,[2,3] and rigidifying the cell.[4,5] OMPs are posttranslationally secreted into and subsequently trafficked through the aqueous periplasm by a network of chaperone proteins that bind to unfolded OMPs (uOMPS) to prevent aggregation and misfolding.[6–8] Folding is finally catalyzed by the β-barrel assembly machine (BAM) at the outer membrane.[9–11] SurA is thought to be the most important chaperone in the OMP biogenesis pathway as it has been shown to interact with a subset of OMPs[12] (termed "clients") at every stage of this pathway: it is associated with OMPs at the translocon during secretion into the periplasm,[13] in the aqueous periplasm,[14] and is thought to hand-off clients to the BAM complex.[15]

Structurally, SurA contains three domains that are connected by flexible linkers including a core chaperone domain comprised of both the N- and C-terminal regions of the sequence, and two peptidyl prolyl isomerase (PPIase) domains, P1 and P2. Figure 1a shows the monomeric crystal structure of SurA in which the P1 domain is bound to the core domain while the P2 domain is extended away from the core-complex.[16] In solution, however, alternative conformations of SurA are thought to exist. Indeed, the chaperone activity of SurA has been linked to the conformational dynamics of its domains, as a mutation at the core-P1 interface was shown to increase chaperone activity in vivo.[17] These data imply an "open" conformation of SurA in which each domain is structurally isolated from the others; this open conformation has subsequently been confirmed as the active, uOMP-binding conformation of SurA.[18,19]

In this work, we investigated the intrinsic properties of SurA in solution to better understand and model SurA function in the uOMP biogenesis pathway. Unlike the other general chaperones in the uOMP biogenesis pathway that form functional oligomers we find that SurA is monomeric in solution at concentrations equivalent to the reported expression level in *Escherichia coli*. Using small-angle neutron scattering (SANS) to examine the hydrodynamic properties of SurA we observe that the radius of gyration is compatible with an average domain organization in which one PPIase domain is unbound and extended away from the two interacting domains. We further used the experimental scattering curve to assess which structural models of SurA are representative of the solution conformation of SurA. This analysis potentially identifies a novel conformation of the P1-closed conformation in which the P1 domain is

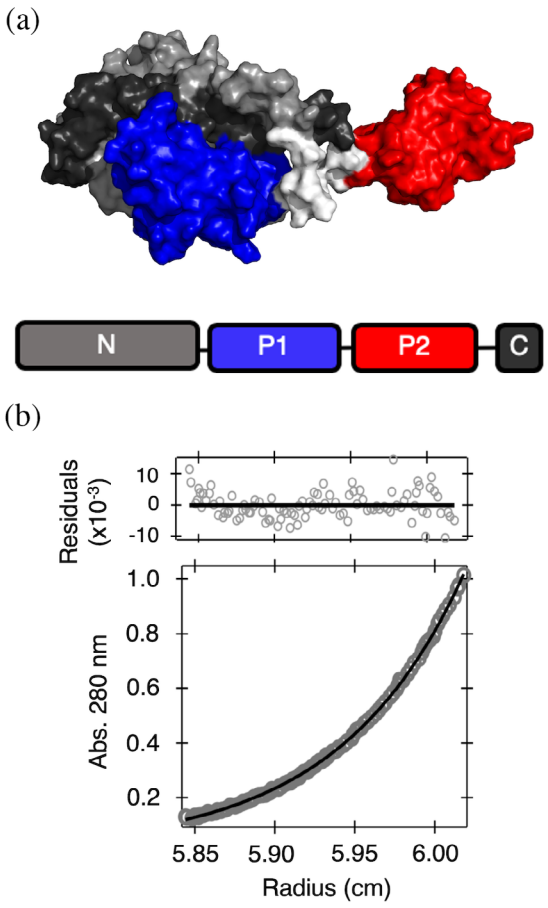

FIGURE 1 SurA is Monomeric in Solution. (a) The monomeric crystal structure of SurA (Protein Data Bank [PDB] ID: 1M5Y) is shown as a surface representation with its domains colored as depicted in the sequence diagram below. The flexible linkers between the domains of SurA are colored white. In this conformation of SurA, the core (N and C regions) and P1 domains are contacting each other, while the P2 domain is extended away in a structurally isolated conformation. (b) Representative sedimentation equilibrium (SE) data set collected for SurA at a total concentration of 25 μM. These data are well described by a single-ideal species model with a molar mass equal to 43 ± 2 kDa. This agrees with the calculated molecular weight of monomeric SurA (45 kDa). These values represent the average weight obtained from fitting three independent experiments and the standard deviation of fitting (Figure S1)

docked to the core domain using an interaction surface not observed in crystal structures. Finally, we measured the energetics associated with PPIase-core domain interactions and discovered that both the P1 and P2 domains compete for binding to the core domain. Together, our results quantify the intrinsic conformational ensemble of SurA and provide insight into a potential mechanism for the regulation of its chaperone function.

2 | RESULTS

2.1 | SurA is monomeric in solution

Many chaperones self-associate to form higher order species that bind to their unfolded client proteins.[20–22] The other general chaperones in the uOMP biogenesis pathway, Skp and FkpA, both use this oligomeric approach to solubilize uOMPs in the periplasm.[23–26] SurA, on the other hand, is thought to exist in a monomeric conformation in the periplasm. However, SurA crystallizes as a dimer when the P2 domain is deleted.[27] It was unclear until now whether full-length SurA can dimerize, and whether a dimeric state is populated at the native concentration of SurA in the periplasm.

To determine the oligomeric state(s) of SurA that exist in solution we measured the apparent molecular weight of wild-type (WT) SurA using analytical ultracentrifugation sedimentation equilibrium (SE). Figure 1b shows that the SE profile for WT SurA is well described by a single-ideal species model corresponding to the molecular mass of the SurA monomer (global fit shown in Figure S1). Notably, this experimental concentration range, that is, 8–25 μmoles/L (μM), encompasses the reported SurA periplasmic concentration (20 μM).[28,29] These results therefore suggest that WT SurA is monomeric under physiological protein concentrations.

2.2 | SurA exists in an expanded conformation in solution

Given that SurA is monomeric in solution, we investigated the structural conformation of SurA in solution to gain insight into how this may affect its function. Specifically, the relative orientation of the domains of SurA has been recently called into question. In the monomeric crystal structure of SurA reported by Bitto and McKay (Protein Data Bank [PDB] ID: 1M5Y) the P2 domain exists in an extended conformation away from the core and P1 domains, which are interacting.[16] We refer to this general domain arrangement as "P1-closed." In contrast to this domain organization, Radford and coworkers recently used a combination of chemical crosslinking and single-molecule Förster resonance energy transfer (smFRET) to show that the P2 domain may exist in a more collapsed conformation in solution.[18]

To address the discrepancy of the overall size and shape of SurA between the two studies, we measured the solution hydrodynamic properties of SurA using SANS. SANS is a label-free method that reports on the intrinsic size and shape of biomolecules in solution. Guinier analysis of the scattering profile of SurA reveals the radius of gyration (R_G) for WT SurA equals 32.8 ± 0.5 Å (Figure 2a, Table S1). This finding agrees with R_G of the monomeric 1M5Y SurA crystal structure calculated using HullRad (33 Å)[30] and indicates that the unbound PPIase domain is located distal from the core-PPIase complex on average.

We next used the entire SANS scattering curve to evaluate whether any of the available 22 structural models of SurA represents the average SANS curve in solution. The available models are derived either from crystal structures or molecular dynamics simulations. Although the monomeric crystal structure R_G agrees with the Guinier region, a reduced χ^2 analysis using the model SANS curve calculated from the monomeric crystal structure (1M5Y) using the SasCalc module in SASSIE[31,32] shows that this crystal conformation is not in fact a good representation of the data as evidenced by the lack of overlay between the predicted and observed scattering curves (Figure 2b), by nonrandom residuals (Figure S2), and by a reduced $\chi^2 = 4.567$ (Table S2) that is significantly elevated above the target value of $\chi^2 \cong 1$ for a good fit. We observed much poorer fits for "open" ($\chi^2 = 10.063$) and "P2-closed" ($\chi^2 = 10.985$) conformations of SurA monomers. The P2-closed conformation has a domain arrangement in which the P2 is bound to the core domain while the P1 domain is extended away from the core-P2 complex, and its existence is implied by the folding studies described below. Finally, 17 of 19 structural models recently published also show poor fits (Table S2) even though these structural models more broadly explore the conformational arrangements of the P1 and P2 domains.[18] Figure 2c depicts a succinct summary of how all 22 structural models describe the data: those with predicted R_G values less than the experimental R_G display large reduced χ^2 values and do not fit the data.

Having eliminated most structural models, we found two published models that describe the experimental SANS curve well (reduced $\chi^2 < 2$). Figure 2b shows the overlay of the SasCalc curve for the best fitting model, termed P1C1 (P1-closed number 1) for which $\chi^2 = 1.536$. Figure 2d shows this structural model oriented similarly to the monomeric crystal structure shown in Figure 1c). Although not shown, both the P1 orientation and the SasCalc curve for the second structure, P1C2 ($\chi^2 = 1.655$)

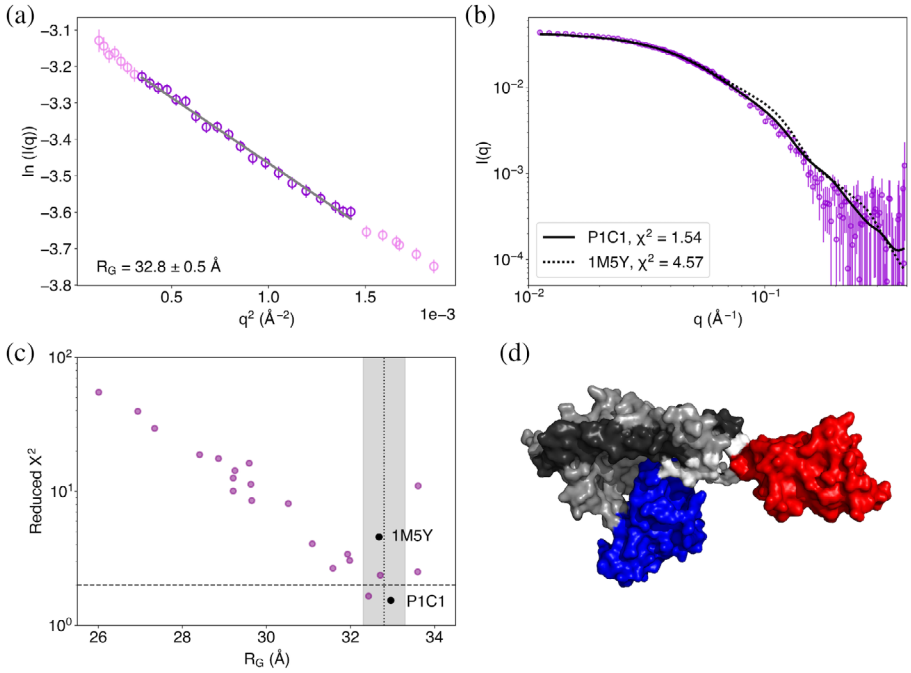

FIGURE 2 Elongated models of SurA best describe small-angle neutron scattering (SANS) curve. (a) The Guinier region of the WT SurA SANS dataset in 98% D_2O is shown, with the data shown in darker purple used to conduct the Guinier analysis. The fit for this region is shown with a gray line, with the radius of gyration obtained from the fit shown at the bottom left corner. Additional $q * R_G$ ranges give similar values and are shown in Table S1. (b) The experimental SANS curve is shown in violet circles with error bars to reflect the standard error of the mean with respect to the number of pixels used in data averaging. The predicted scattering profiles from P1C1 and 1M5Y are shown as solid and dashed lines, respectively. (c) The reduced χ^2 of each available structural model of SurA is plotted against the predicted R_G values calculated using HullRad.[30] Each point is a different conformation of SurA, with reduced χ^2 and R_G values listed in Table S2. The dotted vertical line indicates the R_G value obtained from the Guinier analysis, with the error represented by the shaded gray region. The horizontal dashed line marks a cutoff for a reduced χ^2 of 2. The data points for P1C1 and 1M5Y are shown in black and labeled. (d) The P1C1 structural model is shown as a surface representation and colored as described in Figure 1

are very similar. P1C1 and P1C2 are similar to the monomeric crystal structure in that all three of these can be generally considered as P1-closed conformations because the P2 domain is isolated in solution and the P1 domain is docked onto the core domain. However, the core-P1 interaction in P1C1 is distinct from the monomeric crystal structure: it occurs through a different interface than the crystal structure. In P1C1, the P1 domain has translated and rotated relative to the core domain. Overall, the abilities of these particular SurA conformations to fit the experimental scattering profile better than any other structural model means that a predominantly P1-closed conformation represents the ensemble average structure of SurA in solution.

2.3 | The P1 and P2 domains independently compete for binding to the core domain

To gain insight into the conformational ensemble of SurA, we measured the binding energetics of P1 and P2 domains to the core domain. To access these interaction energies, we first measured the thermodynamic stability of multiple SurA domain-deletion constructs using chemical denaturation titrations. Figure 3 shows that the denaturation titrations of each construct are well described by a two-state, linear extrapolation model.[33] In these titrations, we monitored the urea-dependent change in the circular dichroism (CD) signal at 222 nm, which reports on the foldedness of α-helices. This signal reports primarily on the core domain because it contains the vast majority of the α-helices in SurA (Figure S2). The two-state behavior of every SurA construct further confirms that CD is primarily measuring the folding of just the core domain, as more transitions would be expected in the cases where the PPIase domain unfolding was visualized in our experiments.

These data show that each SurA construct has a different stability. Because our titrations report on the core domain in each construct, these results indicate that the presence of the P1 and P2 domains modulate the stability of the core domain through favorable interactions. The intrinsic interaction energies between the

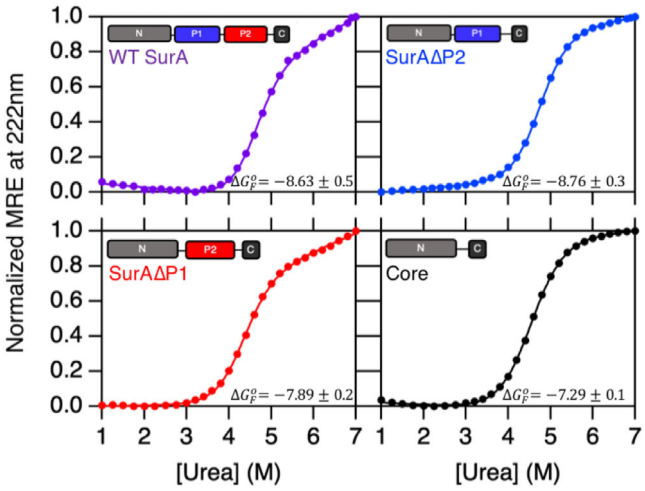

FIGURE 3 Chemical denaturation titrations of SurA domain-deletion constructs. Circular dichroism signal at 222 nm was monitored as a function the concentration of urea to measure the equilibrium unfolding of SurA constructs of varying compositions. The cartoons in the upper left-hand corner of each plot indicate the domain organization of each construct. Each SurA construct was found to cooperatively unfold and were fit to a two-state, linear extrapolation model. The folding stabilities of each construct are shown in the bottom right-hand corner of each plot and are the average of three independent titrations, with errors representing the standard deviation between the three measured stabilities. The WT SurA and SurAΔP2 titrations were best fit with an *m* value of unfolding equal to 1.78 and the SurAΔP1 and core domain titrations were best fit with an *m* value of 1.75, as determined by globally fitting the three titrations for each construct separately

core and PPIase domains can be calculated by taking the difference between the stabilities of the isolated core domain from those of either SurAΔP2 or SurAΔP1, for example, $\Delta G^o_{\mathrm{P1,int}} = \Delta G^o_{F,\mathrm{SurA\Delta P2}} - \Delta G^o_{F,\mathrm{SurA\Delta P1\Delta P2}}$ and $\Delta G^o_{\mathrm{P2,int}} = \Delta G^o_{F,\mathrm{SurA\Delta P1}} - \Delta G^o_{F,\mathrm{SurA\Delta P1\Delta P2}}$. Using this strategy, we find a thermodynamically favorable core-P2 interaction, $\Delta G^o_{\mathrm{P2,int}} = -0.6$ kcal mol^{-1}. This was surprising because an interaction between the core and P2 domain has not been structurally resolved, though recent work suggests that the P2 domain may reside closer to the core domain than in the crystal structure.[18] In contrast, the P1 domain interacts slightly more favorably, $\Delta G^o_{\mathrm{P1,int}} = -1.47$ kcal mol^{-1}, as expected from its docked conformation.

The ability of the P2 domain to bind the core domain raises the question of whether the PPIase domains can both bind the core domain at the same time or if they compete for a single binding site. To address this question, we constructed a thermodynamic cycle of the four SurA domain-deletion constructs as shown in Figure 4. This analysis reveals that both PPIase domains bind the core domain more favorably in the absence of the other PPIase domain. In other words, the presence of the P2 domain affects the apparent affinity of the P1 domain and vice versa. These differences are reflected in the $\Delta G^o_{\mathrm{P1,comp}}$ and $\Delta G^o_{\mathrm{P2,comp}}$ energy terms, and this result means that the P1 and P2 domains compete with each other for a binding site on the core domain. The nature of the competition can be assessed by comparing the

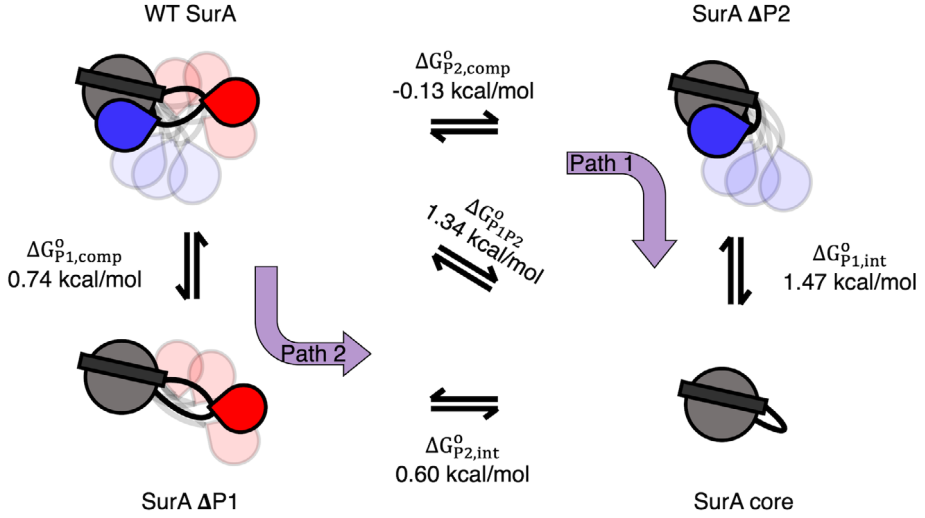

FIGURE 4 Thermodynamic cycle analysis reveals competitive interactions between the peptidyl prolyl isomerase (PPIase) domains and the core. Thermodynamic cycle describing the difference in stabilities between two domain deletion constructs of SurA is shown. The four SurA constructs are shown as cartoons with the most favorable conformation of SurA colored solid and transparent domains to indicate the flexibility of the P1 and P2 domains relative to the core domain. Each side of the cycle is labeled to indicate the corresponding ΔG^o in Table S3. The two indirect thermodynamic paths from WT SurA to the core domain are indicated with purple arrows, and the direct path is indicated with the diagonal arrows in the middle of the cycle. This analysis reveals that the P1 and P2 domains compete for binding to the core domain in a thermodynamically uncoupled manner. This mechanism necessitates three conformations of SurA

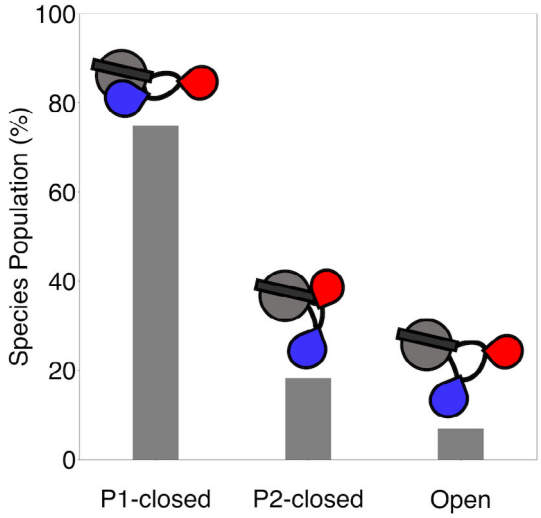

FIGURE 5 The relative populations of the three conformations of SurA. Cartoon models of each conformation is shown above the bar. The percent population of each conformation in solution was calculated using $\Delta G^{o}_{P1,int}$ and $\Delta G^{o}_{P2,int}$

summed free energy changes along the two paths from the WT SurA (top-left corner of the cycle) to the isolated core domain (bottom-right corner). Figure 4 demonstrates that these two paths (curved arrows) are energetically equivalent. Therefore, there is no evidence for allosteric communication between the P1 and P2 domains, and we conclude from these data that the two microscopic binding events are thermodynamically uncoupled and thus independent.

The observation of independent, competitive binding of the P1 and P2 domains to a single site on the core domain necessitates that at least three distinct conformations of SurA exist in solution. Figure 5 shows the distribution of these populations at equilibrium calculated from the interaction energies. The dominant conformation (75%) is P1-closed and the second most favorable conformation (18%) is P2-closed. To switch between these two conformations, an "open" conformation where both the P1 and P2 domains are structurally isolated from the core domain must exist in the remaining 7% of the population of the SurA conformational ensemble. These equilibrium populations are in agreement with the SANS data that revealed the P1C1 P1-closed conformation to be most represented of the average ensemble in solution.

3 | DISCUSSION

SurA is a key member of the periplasmic chaperone network in the OMP biogenesis pathway in gram-negative bacteria. The other chaperones in this network, Skp and FkpA, oligomerize to sequester uOMPs to prevent their aggregation and shield them from interacting with other proteins.[25,34–38] In contrast, we find that SurA does not oligomerize in solution at physiological concentrations. This means that SurA does not adopt a structural organization that encapsulates uOMP clients, consistent with the distinct roles that SurA plays in the OMP biogenesis pathway compared to Skp and FkpA. Unlike these chaperones, evidence suggests SurA delivers uOMPs to the BAM complex to initiate their folding.[15] Additionally, recent work has shown that SurA can interact with uOMPs as they are secreted into the periplasm through the translocon.[13] These auxiliary functions require a binding mode in which SurA can protect the client uOMPs while allowing for uOMPs to interact with other proteins in the biogenesis pathway.

Indeed, the conformational dynamics of SurA have been proposed to regulate and promote binding of client uOMPs.[18] In particular, mutations affecting the core-P1 interaction increase the apparent chaperone activity of SurA in vivo,[17] and the transition between the "P1 closed" and "open" conformations has been shown be necessary for uOMP binding. Using equilibrium thermodynamics, we have found that both the P1 and P2 domains compete for binding to the core domain. This competition results in 93% of the SurA molecules existing in a conformation in which one of the PPIase domains of SurA occupies the proposed uOMP binding site. Therefore, the P1 and P2 domains inhibit the exposure of the client-binding site on SurA in the absence of uOMPs. As SurA is thought to only bind a subset of OMPs,[14] we speculate this inhibitory function may serve to prevent SurA from binding nonclient uOMPs or other proteins in the periplasm. Interestingly, this autoinhibition does not appear to be allosterically regulated, although it should be noted that our work does not exclude cooperative coupling in the presence of a client uOMP. Further structural studies will be required to evaluate the details of whether there is a single binding site or two overlapping binding sites for the P1 and P2 domains on the core domain.

Finally, we investigated the intrinsic hydrodynamic properties of SurA, as the conformation adopted by the unbound PPIase domain (usually P2) may be important for the function of SurA. We find that the R_G of SurA in solution is approximately equal to that of a "P1-closed" domain arrangement in which the P2 domain must also be extended away from the core-P1 complex. Our finding is seemingly in conflict with recent work that concluded that the P2 domain exists in a more collapsed state.[18] This contradiction can be resolved by recognizing that the latter conclusions were primarily based on the ability of the P2 domain to chemically crosslink with the core and P1 domains and on smFRET experiments measuring apparent distances between domains. While the presence of

crosslinks confirms that the P2 can exist in a collapsed conformation, one drawback is that these data do not report on the relative populations. Moreover, Sosnick and coworkers have shown that the fluorescent dyes attached to intrinsically disordered proteins in smFRET experiments can lead to reduced hydrodynamic sizes as compared label-free methods, such as scattering.[39] Because the P2 domain is connected to the core and P1 domains by flexible linkers, it is reasonable to expect the published smFRET data may overestimate the compaction of the P2 domain in solution. Our SANS-based R_G was obtained in the absence of exogenous modifications of SurA and therefore is a more accurate measurement of the intrinsic size of SurA in solution. Together, the data support a model where the position of the P2 domain relative to the core-P1 complex is highly dynamic with its average position being found in an extended conformation.

Using the full SANS scattering curves, we identified the P1C1 conformation of SurA as best representing the average conformation of SurA in solution. In this structural model the P2 domain is structurally expanded away from the core-P1 complex. The P1 domain in these models is contacting the core domain, but in a location that is different from the canonical monomeric crystal structure. This raises the idea that the PPIase domain binding site on the core domain may be larger than previously indicated from structural studies. The location of the P1 domain in these models warrants further investigation, as it may provide insight into biologically important SurA conformations.

By quantifying the dynamics and energetics that determine the intrinsic conformational ensemble of SurA, we can begin to understand exactly how SurA recognizes uOMPs in the periplasm. In conclusion, we have determined that SurA exists as monomer in solution in a slightly expanded conformation where its PPIase domains compete for binding to the core domain. Paradoxically this dynamic conformational ensemble reduces the population of the chaperone-active, "open" conformation in the absence of client uOMPs. On the other hand, autoinhibition has the advantage of increasing discrimination of SurA for its clients and for preserving the reservoir of apo-SurA in the periplasm.

4 | MATERIALS AND METHODS

4.1 | SurA construct cloning

The WT SurA plasmid was designed by inserting the *Escherichia coli* gene for SurA with a C-terminal 6-Histidine tag into the pET28b vector between restriction sites Nde I and BamHI. The signal sequence was omitted from the sequence for cytoplasmic expression. Primers for SurAΔP1 and core domain constructs were designed using the Takara Infusion primer design website tool (https://takara.teselagen.com/#/DesignPage). These two constructs were cloned using the In-Fusion HD Cloning Plus CE method (Takara). SurAΔP2 was created through a multi-step approach in which both the first 281 amino acids of SurA were amplified (N and P1 domains) and the region starting with residue 383 until the end of the sequence were amplified. These two fragments were joined and amplified using polymerase chain reaction, followed by insertion into a linearized pET-28b vector using Gibson assembly. All primers used to create SurA constructs are listed in Table S4.

Stellar cells were transformed with the PCR product by heat shock and plated grown overnight on Luria Broth plates with 50 μg/ml kanamycin at 37°C. Plasmid DNA was extracted from single colonies with the GeneJET Plasmid Miniprep Kit and sequenced to validate the construct sequences. Plasmids were transformed into *E. coli* HMS174(DE3) via electroporation for protein expression and stored at −80°C as glycerol stocks.

4.2 | SurA expression and purification

Terrific broth (TB) cultures of 5 ml containing 50 μg/ml kanamycin were inoculated with cells containing a SurA plasmid and grown overnight at 37°C. These cultures were used to inoculate a 500-ml TB culture with antibiotics at 37°C and were grown until reaching an OD_{600} of 0.6–0.8, followed by addition of isopropyl-β-D-1-thiogalactopyranoside (IPTG) to induce expression our constructs overnight. Cells containing SurA FL and SurA ΔP2 plasmids were expressed at 37°C, while cells containing plasmids encoding for SurA ΔP1 and the isolated core domain were expressed at room temperature. For all growths, cells were pelleted by centrifugation at 5,000 rpm (rpm = 1/60 Hz) for 15 min (Beckman J2-MI, JA-10 rotor) the following morning and stored at −20°C.

Cells were thawed for lysis and then solubilized in 25 ml of Buffer A (20 mM sodium phosphate, 500 mM NaCl, 20 mM imidazole, pH 8.0) containing a ethylenediaminetetraacetic acid (EDTA)-free protease inhibitor tablet (Pierce). An Emulsiflex homogenizer (Avestin) was used to lyse cells, followed by centrifugation (Beckman J2-MI, JA-10 rotor) for 30 min at 5,500 rpm to pellet cell debris. Clarified cell lysate was passed through a 0.45-μM Millex filter prior to being loaded onto to a Ni-NTA sepharose high-performance bench-top column that was preequilibrated with Buffer A. The column was then washed with 40 ml of Buffer A, followed by elution with 30 ml of Buffer B (Buffer A

+ 300 mM imidazole). A second round of protein purification was performed using FPLC with a Superdex 75 Increase 10/300 GL column (GE) in an elution buffer of 20 mM Tris–HCl, pH 8.0. The purity of elution fractions was assessed by sodium dodecyl sulfate polyacrylamide gel electrophoresis (SDS-PAGE) and protein concentration was assessed using the theoretical extinction coefficient 29,450 M/cm. SurA stocks were stored at −20°C until experiments were performed.

4.3 | SE analytical ultracentrifugation

SE analytical ultracentrifugation experiments were used to evaluate the oligomerization state of SurA in solution. SurA was diluted into three samples with $A_{280} = 0.90$, 0.60, and 0.30 at a path length of 1.2 cm (corresponding to concentrations of 25, 17, and 8 μM, respectively) in 20 mM Tris buffer (pH = 8.0). Samples were loaded into six-sector centerpieces and allowed to equilibrate at speeds of 20,000, 24,500, and 30,000 rpm in a Beckman Optima XL-A analytical ultracentrifuge with absorbance optics. Data were collected at 37°C with radial scans (wavelength, $\lambda = 280$ nm) acquired with 0.001 cm radial steps with 10 replicates. The condition of sedimentation equilibration was confirmed using WinMatchv0.99, and data were subsequently trimmed using WinReedit v.0999.0028 to regions where Beer's law applies.[40] Global fitting was completed utilizing WinNonLin v.1.06.[40] For data analysis, we calculated partial-specific volume values and buffer densities using Sednterp v.20130813b.[41] The values used for protein partial specific volume ($\bar{\nu}$) is: $\bar{\nu} = 0.7325$ ml/g. For 20 mM Tris buffer (pH = 8.0), the buffer density (ρ) and buffer viscosity (η) are $\rho = 0.9988$ g/ml and $\eta = 1.0069$ mPa.

4.4 | SANS of WT SurA

All scattering experiments were collected at the National Institute of Standards and Technology Center for Neutron Research (Gaithersburg, MD) as previously described.[23] The scattering data presented here were collected on the NGB 30-m SANS Instrument (National Institute of Standards and Technology [NIST]). A neutron beam of wavelength $\lambda = 6$ Å (wavelength spread, $\Delta\lambda/\lambda = 0.15$) was utilized to collect scattering profiles from all samples described here on a 2D position-sensitive detector (64 cm × 64 cm) with 128 × 128 pixels at resolution of 0.5 cm pixel^{-1}. For data processing, raw counts were normalized to a common monitor count and then corrected for empty cell counts, ambient room background counts, and non-uniform detector response. Data were placed on an absolute scale by normalizing the scattering intensity to the incident beam flux for each individual pixel. Radial averaging was utilized to produce scattering intensity profiles, $I(q)$ versus q; $q = 4\pi\sin(\theta)/\lambda$, where 2θ is the scattering angle, λ is the neutron wavelength, and q is the magnitude of the scattering vector. Sample-to-detector distances of 5.0 and 1.5 m were used to cover a range of 0.01 Å^{-1} < q < 0.4 Å^{-1}.

We prepared the WT SurA protein with a slightly modified protocol for SANS analysis. After expression and purification in that we further purified SurA by gel-filtration (GF) in 20 mM Tris and 200 mM NaCl (pH = 8.0, GF buffer). SurA (40 μM) was injected onto a Superdex 200 10/300 (GE Healthcare Life Sciences) gel-filtration column in GF buffer with a flow rate of 0.6 ml/min. Fractions containing SurA were pooled and buffer exchanged into GF buffer containing 98% D_2O via centrifugation in an Amicon filter (Millipore) with a 10-kDa molecular weight cut-off. We collected the scattering profile of apo-SurA at 1 mg/ml (20 μM).

For initial analysis of SANS data, we utilized the Guinier approximation to obtain two fit parameters: the macromolecule R_G (Å) and the forward scattering intensity at $q = 0$ (i.e., I[0] in cm^{-1}). This approximation estimates the intensity in low q regions as follows:

$$I(q) \approx I(0)\exp\left[-\left(\frac{1}{3}\right)R_G^2 q^2\right], \quad (1)$$

$$\ln[I(q)] \approx \ln[I(0)] - \frac{1}{3}R_G^2 q^2. \quad (2)$$

Therefore, linear regression of ln[($I(q)$] versus q^2 yields information in the slope (i.e., R_G^2) and the intercept (i.e., $I(0)$). $I(0)$ was also calculated using the contrast calculator module[42] in the web version of the SASSIE software developed at NIST[32]:

$$I(0) = \frac{C\Delta\rho^2\bar{\nu}^2 M}{N_A}. \quad (3)$$

In the above equation, C indicates the protein concentration in mg/ml, $\Delta\rho$ is the contrast, $\bar{\nu}$ is the protein partial-specific volume in ml/g, M is the molecular weight in Da, and N_A is Avogadro's number. We compared the fit value of $I(0)$ to the calculated value to ensure that samples contain homogeneous, monomeric species (Table S1).

4.5 | SANS SasCalc calculations

This module requires several input parameters to be specified including PDB files to indicate atom positions,

buffer (H_2O:D_2O) composition, protein deuteration level and $I(0)$ value. For SasCalc, we built the missing linkers/loops and a C-terminal histidine tag onto 1M5Y using Modeller.[43] We created the open conformation by combining the core-P1 domain arrangement from 2PV3[27] and the core-P2 domain arrangement from 1M5Y. The P2-closed conformation was built by taking the open conformation and collapsing P2 to the binding groove between the core and P1 domains.

4.6 | Evaluation for agreement between SANS data and structural models

The SasCalc module in SASSIE was used to calculate SANS profiles ($P(q)_{calc}$) for all structural models.[31,32] SasCalc curves were evaluated for their ability to describe the experimental SANS curve using the reduced χ^2 as recommended by Trewhella and colleagues[44]:

$$\chi^2 = \frac{1}{N-1}\sum_{1}^{N}\left[\frac{I(q)_{obs} - I(q)_{calc}}{\sigma_{obs}}\right]^2, \quad (4)$$

where N equals the number of data points, $I(q)_{obs}$ and $I(q)_{calc}$ are the experimental and calculated intensity values, respectively, at each point q and σ_{obs} is the error on the experimental measurement at each point. A good fit is defined as $\chi^2 = 1$.

4.7 | CD urea titrations

CD titrations were collected on an Aviv 62A DS spectropolarimeter using a 0.1 cm quartz cuvette. SurA and domain deletion constructs were diluted to 1 μM (SurA, SurAΔP1, SurAΔP2) or 1.5 μM (core) in buffer containing 20 mM Tris (Fisher Scientific), pH 8.0. Equilibrium unfolding titrations were conducted by titrating a solution containing equivalent protein concentration to the analyte and 8 M urea (ThermoFisher), 20 mM Tris, pH 8.0 using a computer-controlled titrator (Hamilton) to maintain constant protein concentration. Each urea step was between 0.1 and 0.2 M urea until a final concentration of 7 M urea was reached, with 5 min of equilibration time with stirring between each reading. Signal at 222 nm was averaged at each data point 30 s with stirring off. Three repeats were conducted for each construct.

We then used a two-state linear extrapolation model[45] to fit the normalized titration curves with the equation below:

$$Y_{obs} = \frac{(Y_N + a_N[\text{Urea}]) + (Y_U + a_U[\text{Urea}]) * e^{-\left(\frac{\Delta G^o_{N-U} + m[\text{Urea}]}{RT}\right)}}{1 + e^{-\left(\frac{\Delta G^o_{N-U} + m[\text{Urea}]}{RT}\right)}}, \quad (5)$$

where Y_{obs} is the observed signal; Y_N and Y_U are the intercepts of the native and unfolded baselines, respectively; a_N and a_U are the slopes of the folded and unfolded baselines, respectively; m_T is the m value, [Urea] is the concentration of urea, ΔG^o_{N-U} is the change in Gibbs free energy of folding, R is the gas constant, and T is the temperature (393 K). The m value was determined by globally fitting all three repeats: m = 1.78 for SurA and SurAΔP2, m = 1.75 for SurAΔP1 and SurA core. Mean and SD values were calculated for the ΔG values of each construct.

ACKNOWLEDGMENTS

We thank the Center for Molecular Biophysics for providing facilities and resources. We also thank Kathryn Weaver for help cloning the SurAΔP2 construct. Access to NGB30 SANS was provided by the Center for High Resolution Neutron Scattering, a partnership between the National Institute of Standards and Technology and the National Science Foundation under Agreement No. DMR-1508249. We acknowledge the support of the National Institute of Standards and Technology, U.S. Department of Commerce, in providing the neutron research facilities used in this work. This work benefitted from CCP-SAS software developed through a joint EPSRC (EP/K039121/1) and NSF (CHE-1265821) grant. This work was supported by National Science Foundation (NSF) grants MCB1412108 and MCB1931211. Dagan C. Marx and Ashlee M. Plummer were supported by NIH training grant T32 GM008403. Ashlee M. Plummer was supported by the NSF grant DGE 1232825. Mathis J. Leblanc was supported by a Krieger School of Arts and Sciences Aspire Award. The authors thank lab members for helpful discussions. Certain commercial equipment, instruments, or materials (or suppliers, or software, etc.) are identified in this paper to foster understanding. Such identification does not imply recommendation or endorsement by the National Institute of Standards and Technology, nor does it imply that the materials or equipment identified are necessarily the best available for the purpose.

CONFLICT OF INTEREST

The authors declare no potential conflict of interest.

AUTHOR CONTRIBUTIONS

Dagan Marx: Conceptualization; data curation; formal analysis; methodology; project administration; supervision; visualization; writing-original draft; writing-review and editing. **Mathis Leblanc:** Conceptualization; data curation; formal analysis; visualization; writing-original draft; writing-review and editing. **Ashlee Plummer:** Conceptualization; formal analysis; investigation; visualization; writing-review and editing. **Susan Krueger:** Conceptualization; data curation; formal analysis; investigation; methodology; writing-review and editing. **Karen Fleming:** Conceptualization; data curation; formal analysis; funding acquisition; investigation; supervision; visualization; writing-original draft; writing-review and editing.

ORCID

Karen G. Fleming https://orcid.org/0000-0001-5417-8830

REFERENCES

1. Noinaj N, Guillier M, Barnard TJ, Buchanan SK. TonB-dependent transporters: Regulation, structure, and function. Ann Rev Microbiol. 2010;64:43–60.
2. Bishop RE. Structural biology of membrane-intrinsic β-barrel enzymes: Sentinels of the bacterial outer membrane. Biochim Biophys Acta Biomembr. 2008;1778:1881–1896.
3. Bishop RE. The lipid A palmitoyltransferase PagP: Molecular mechanisms and role in bacterial pathogenesis. Mol Microbiol. 2005;57:900–912.
4. Lessen HJ, Fleming PJ, Fleming KG, Sodt AJ. Building blocks of the outer membrane: Calculating a general elastic energy model for β-barrel membrane proteins. J Chem Theory Comput. 2018;14:4487–4497.
5. Rojas ER, Billings G, Odermatt PD, et al. The outer membrane is an essential load-bearing element in gram-negative bacteria. Nature. 2018;559:617–621.
6. Chum AP, Shoemaker SR, Fleming PJ, Fleming KG. Plasticity and transient binding are key ingredients of the periplasmic chaperone network. Protein Sci. 2019;28:1340–1349.
7. Costello SM, Plummer AM, Fleming PJ, Fleming KG. Dynamic periplasmic chaperone reservoir facilitates biogenesis of outer membrane proteins. Proc Natl Acad Sci USA. 2016;113:E4794–E4800.
8. Plummer AM, Fleming KG. From chaperones to the membrane with a BAM! Trends Biochem Sci. 2016;41:872–882.
9. Ricci DP, Silhavy TJ. Outer Membrane Protein Insertion by the β-barrel Assembly Machine. EcoSal Plus. 2019;4:1–9. https://doi:10.1128/ecosalplus.ESP-0035-2018.
10. Wu R, Stephenson R, Gichaba A, Noinaj N. The big BAM theory: An open and closed case? Biochim Biophys Acta Biomembr. 2020;1862:183062.
11. Plummer AM, Fleming KG. BamA alone accelerates outer membrane protein folding in vitro through a catalytic mechanism. Biochemistry. 2015;54:6009–6011.
12. Denoncin K, Schwalm J, Vertommen D, Silhavy TJ, Collet J-F. Dissecting the *Escherichia coli* periplasmic chaperone network using differential proteomics. Proteomics. 2012;12:1391–1401.
13. Alvira S, Watkins DW, Troman L, et al. Trans-membrane association of the Sec and BAM complexes for bacterial outer-membrane biogenesis. bioRxiv. 2020;1–65. https://doi.org/10.1101/589077.
14. Vertommen D, Ruiz N, Leverrier P, Silhavy TJ, Collet J-F. Characterization of the role of the *Escherichia coli* periplasmic chaperone SurA using differential proteomics. Proteomics. 2009;9:2432–2443.
15. Wang Y, Wang R, Jin F, et al. A supercomplex spanning the inner and outer membranes mediates the biogenesis of β-barrel outer membrane proteins in bacteria. J Biol Chem. 2016;291:16720–16729.
16. Bitto E, McKay DB. Crystallographic structure of SurA, a molecular chaperone that facilitates folding of outer membrane porins. Structure. 2002;10:1489–1498.
17. Soltes GR, Schwalm J, Ricci DP, Silhavy TJ. The activity of *Escherichia coli* chaperone SurA is regulated by conformational changes involving a parvulin domain. J Bacteriol. 2016;198:921–929.
18. Calabrese AN, Schiffrin B, Watson M, et al. Inter-domain dynamics in the chaperone SurA and multi-site binding to its outer membrane protein clients. Nat Commun. 2020;11:2155.
19. Marx DC, Plummer AM, Faustino AM, et al. SurA is a "groove-y" chaperone that expands unfolded outer membrane proteins. bioRxiv. 2019:1–33. https://doi.org/10.1101/2019.12.17.878660.
20. Stengel F, Baldwin AJ, Painter AJ, et al. Quaternary dynamics and plasticity underlie small heat shock protein chaperone function. Proc Natl Acad Sci USA. 2010;107:2007–2012.
21. Giese KC, Vierling E. Changes in oligomerization are essential for the chaperone activity of a small heat shock protein in vivo and in vitro. J Biol Chem. 2002;277:46310–46318.
22. Liu L, Chen J, Yang B, Wang Y. Oligomer-dependent and -independent chaperone activity of sHsps in different stressed conditions. FEBS Open Biol. 2015;5:155–162.
23. Zaccai NR, Sandlin CW, Hoopes JT, et al. Deuterium labeling together with contrast variation small-angle neutron scattering suggests how Skp captures and releases unfolded outer membrane proteins. Methods Enzymol. 2016;566:159–210.
24. Thoma J, Burmann BM, Hiller S, Müller DJ. Impact of holdase chaperones Skp and SurA on the folding of β-barrel outer-membrane proteins. Nat Struct Mol Biol. 2015;22:795–802.
25. Saul FA, Arié JP, Vulliez-le Normand B, Kahn R, Betton JM, Bentley GA. Structural and functional studies of FkpA from *Escherichia coli*, a cis/trans peptidyl-prolyl isomerase with chaperone activity. J Mol Biol. 2004;335:595–608.
26. Ge X, Lyu ZX, Liu Y, et al. Identification of FkpA as a key quality control factor for the biogenesis of outer membrane proteins under heat shock conditions. J Bacteriol. 2014;196:672–680.
27. Xu X, Wang S, Hu YX, McKay DB. The periplasmic bacterial molecular chaperone SurA adapts its structure to bind peptides in different conformations to assert a sequence preference for aromatic residues. J Mol Biol. 2007;373:367–381.
28. Arike L, Valgepea K, Peil L, Nahku R, Adamberg K, Vilu R. Comparison and applications of label-free absolute proteome quantification methods on *Escherichia coli*. J Proteomics. 2012;75:5437–5448.
29. Masuda T, Saito N, Tomita M, Ishihama Y. Unbiased quantitation of *Escherichia coli* membrane proteome using phase transfer surfactants. Mol Cell Proteomics. 2009;8:2770–2777.

30. Fleming PJ, Fleming KG. HullRad: Fast calculations of folded and disordered protein and nucleic acid hydrodynamic properties. Biophys J. 2018;114:856–869.
31. SASSIE-Web. https://sassie-web.chem.utk.edu/sassie2/.
32. Curtis JE, Raghunandan S, Nanda H, Krueger S. SASSIE: A program to study intrinsically disordered biological molecules and macromolecular ensembles using experimental scattering restraints. Comput Phys Commun. 2012;183:382–389.
33. Santoro MM, Bolen DW. Unfolding free energy changes determined by the linear extrapolation method. 1. Unfolding of phenylmethanesulfonyl alpha-chymotrypsin using different denaturants. Biochemistry. 1988;27:8063–8068.
34. Sandlin CW, Zaccai NR, Fleming KG. Skp trimer formation is insensitive to salts in the physiological range. Biochemistry. 2015;54:7059–7062.
35. Zaccai NR, Sandlin CW, Hoopes JT, et al. Deuterium labeling together with contrast variation small-angle neutron scattering suggests how Skp captures and releases unfolded outer membrane proteins. Methods Enzymol. 2016;566:159–210.
36. Burmann BM, Wang C, Hiller S. Conformation and dynamics of the periplasmic membrane-protein-chaperone complexes OmpX-Skp and tOmpA-Skp. Nat Struct Mol Biol. 2013;20:1265–1272.
37. Walton TA, Sandoval CM, Fowler CA, Pardi A, Sousa MC. The cavity-chaperone Skp protects its substrate from aggregation but allows independent folding of substrate domains. Proc Natl Acad Sci USA. 2009;106:1772–1777.
38. Ramm K, Pluckthun A. The periplasmic *Escherichia coli* peptidylprolyl cis,trans-isomerase FkpA. II. Isomerase-independent chaperone activity in vitro. J Biol Chem. 2000;275:17106–17113.
39. Riback JA, Bowman MA, Zmyslowski AM, Plaxco KW, Clark PL, Sosnick TR. Commonly used FRET fluorophores promote collapse of an otherwise disordered protein. Proc Natl Acad Sci USA. 2019;116:8889–8894.
40. Johnson ML, Correia JJ, Yphantis DA, Halvorson HR. Analysis of data from the analytical ultracentrifuge by nonlinear least-squares techniques. Biophys J. 1981;36:575–588.
41. Laue TM, Shah BD, Ridgeway TM, Pelletier SL. Computer-aided interpretation of analytical sedimentation data for proteins. In: Harding S, Rowe A, Hoarton J, editors. Analytical Ultracentrifugation in Biochemistry and Polymer Science. Cambridge, UK: Royal Society of Chemistry, 1992; p. 90.
42. Sarachan KL, Curtis JE, Krueger S. Small-angle scattering contrast calculator for protein and nucleic acid complexes in solution. J Appl Cryst. 2013;46:1889–1893.
43. Fiser A, Do RKG, Šali A. Modeling of loops in protein structures. Protein Sci. 2000;9:1753–1773.
44. Trewhella J, Duff AP, Durand D, et al. 2017 Publication guidelines for structural modelling of small-angle scattering data from biomolecules in solution: An update. Acta Cryst. 2017; D73:710–728.
45. Bolen DW, Santoro MM. Unfolding free energy changes determined by the linear extrapolation method. 2. Incorporation of Ag°n_u values in a thermodynamic cycle. Biochemistry. 1988; 27:8069–8074.

SUPPORTING INFORMATION

Additional supporting information may be found online in the Supporting Information section at the end of this article.

How to cite this article: Marx DC, Leblanc MJ, Plummer AM, Krueger S, Fleming KG. Domain interactions determine the conformational ensemble of the periplasmic chaperone SurA. *Protein Science*. 2020;29:2043–2053. https://doi.org/10.1002/pro.3924